Experimental demonstration of the band compression effect in engineered kagome-honeycomb lattices

R. G. Yan,[1] T. Z. Ji,[1] W. L. Fan,[1] Z. X. Zhang,[1] H. T. Li,[1] L. Sun,[1,2] B. F. Miao,[1,2] G. Chen,[1,2] and H. F. Ding[1,2,*]

[1]*National Laboratory of Solid State Microstructures and Department of Physics, Nanjing University, Nanjing 210093, China*

[2]*Collaborative Innovation Center of Advanced Microstructures, Nanjing 210093, China*

(Received 16 March 2023; revised 10 July 2023; accepted 4 August 2023; published 22 August 2023)

Utilizing a low-temperature scanning-tunneling microscope, we construct Fe kagome-honeycomb lattices on Ag(111) and investigate their lattice parameter dependent electronic properties. The probed spectra exhibit the characteristic lattice peaks, which gradually merge and form a flat-band peak with decreasing the ratio of the high-order and first nearest-neighbor (NN) hopping, in line with the tight-binding calculations. The one-to-one correspondence unambiguously demonstrates a nontrivial band compression effect by minimizing the high-order NN hopping. Our result provides an efficient approach to realizing flat bands and engineering the electronic properties with artificial structures.

DOI: 10.1103/PhysRevB.108.075153

I. INTRODUCTION

A flat band refers to a dispersionless band where the energy is independent of the momentum. It exhibits a flat-plane/line feature in a three-dimensional/two-dimensional (3D/2D) band structure, respectively. Perfectly flat bands are usually not stable against generic perturbations and become dispersive [1]. Thus, the concept of flat bands is further extended to include partial flat bands that have vanishing dispersion only along specific directions or in the vicinity of special points of the Brillouin zone [2–4]. In an electronic flat band, the effective mass of the electrons increases sharply and the group velocity vanishes. The kinetic energy is therefore quenched, making the system very sensitive to perturbations since their energies can easily dominate over the kinetic energy. This results in a series of novel and strongly correlated quantum phenomena. For instance, the existence of ferromagnetism in Lieb lattices is predicted via Hubbard models [5–7]. High-temperature fractional quantum Hall state is also predicted in kagome flat-band systems [8,9]. Correlated insulating states and tunable superconductivity are observed in the trilayer graphene moiré superlattices [10], magic-angle graphene superlattices [11–13], and twisted bilayer transition metal dichalcogenides [14]. Moreover, owing to their very high sensitivity to perturbations, flat-band systems are believed to play key roles in designing exotic quantum devices and thus are highly desired.

There are several routes for realizing flat-band systems [13,15–22]. Among them, the geometry-induced destructive quantum interference approach is appealing as several simple but interesting lattices are predicted to hold topologically nontrivial flat bands, such as the dice lattice [23], Lieb lattice [5], checkerboard lattice [24,25], kagome lattice, etc. [26–28]. These systems are hotly pursued experimentally, not only in 2D lattices but also in 3D crystals containing such lattices [29–36]. For instance, Lieb and honeycomb lattices with confined electrons on Cu(111) [37,38] and Fe adatoms on Ag(111) [39] have been successfully assembled. Kagome lattices have been realized by trapping potassium atoms into phosphorus-gold potential valleys [40] and by twisting multilayer silicene [20]. More recently, an artificial kagome-honeycomb lattice was constructed by the self-assembly of circumcoronene molecules [41]. Note that the originally predicted flat bands in these lattices only considered the first nearest-neighbor (NN) interaction. Recent calculations showed that these bands are no longer flat and become dispersive when the high-order NN hopping is non-negligible [42,43]. This triggers the possibility that the previously observed experimental peaks in the energy spectra might not be sufficient to confirm a flat band. Moreover, the theoretically calculated influence of the high-order NN hopping on the band structure also needs to be verified experimentally.

In this paper, we employed a low-temperature scanning-tunneling microscope to construct kagome-honeycomb lattices with Fe adatoms on Ag(111). This approach takes advantage of the low-temperature environment and the high spatial and energy resolution. In particular, with atomic manipulation, the free positioning of the adatoms on the surface allows controlling the interatomic distance at the atomic level. With the recently obtained interatomic distance-dependent overlap energy (hopping term) [39], we are able to control the different orders of NN hopping terms in a designed manner. We acquired the scanning-tunneling spectra, investigated the lattices' electronic band characteristics as the function of the ratio of the high-order and first NN hopping terms, and compared the results with the tight-binding calculations. We discovered a nontrivial band compression phenomenon via tuning this ratio, which merges the dispersive bands into flat bands. This is further supported by the one-to-one correspondence between experiments and the tight-binding calculations. Our findings not only reveal a band compression effect but also provides an effective approach to realizing the flat band.

*Corresponding author: hfding@nju.edu.cn

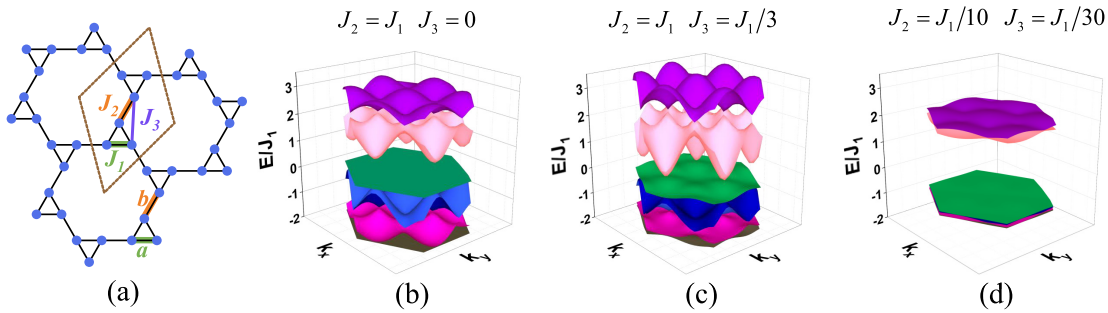

FIG. 1. (a) Sketch of a kagome-honeycomb lattice with the first three order hopping terms: J_1, J_2, and J_3, respectively. a and b represent the side length of the triangles and the lateral shift between two head-to-head triangles, respectively. A unit cell (brown dotted line) contains six sites, indicated by blue dots. (b)–(d) Calculated band structure with the corresponding hopping terms marked on top of the panels. Note: the flat bands are present in (b) and (d) but absent in (c).

It further verifies the significant influence of the high-order NN hopping on the electronic band structure. In addition, the approach also demonstrates the promising capability to engineer the electronic band structure with artificial structures.

II. RESULTS AND DISCUSSIONS

We choose kagome-honeycomb lattices in our study as they not only inherit the exotic electronic band structures from both the kagome and the honeycomb lattices [41,44,45] but also offer the possibility to tune the ratio between the first- and high-order NN distances, which will be discussed below. Figure 1(a) shows a sketch of a typical kagome-honeycomb lattice. It can be understood as the shifting of one of the neighboring honeycombs with a along the edge direction or the splitting of the two head-to-head triangles of a kagome lattice with b along one of the triangle edges. As the hopping term is typically interatomic distance dependent, the ratio between the high-order and first-order NN hopping can be adjusted by tuning the ratio of a/b. The brown dashed line marks the unit cell. J_1 (green), J_2 (orange), and J_3 (purple) represent the corresponding hopping terms, respectively. With these hopping terms, the electronic band structure of the lattice and the local density of states (LDOS) can be readily derived by the following Hamiltonian (see Supplemental Material Note 1 [46]):

$$H = \sum_i \mu_i c_i^\dagger c_i - J_1 \sum_{i,j}^{\text{1st NN}} (c_i^\dagger c_j + \text{H.c.}) - J_2 \sum_{i,j}^{\text{2nd NN}} (c_i^\dagger c_j + \text{H.c.}) - J_3 \sum_{i,j}^{\text{3rd NN}} (c_i^\dagger c_j + \text{H.c.}),$$

where μ_i denotes the on-site energy. They are temporarily set to 0 for clarity and their effects will be discussed in the comparison with the experiments. When $J_2 = J_1$ and $J_3 = 0$, the band structure exhibits two perfect flat bands at $E = 0$ and $E/J_1 = -2$ as shown in Fig. 1(b). These bands, however, can be strongly influenced by J_3 and become dispersive. A typical example is illustrated in Fig. 1(c) for $J_3 = J_1/3$. This is similar to the influence of the second-order NN hopping on the band structure reported in the Lieb and kagome lattices [38,39,42,43]. Remarkably, we find an exotic band compression phenomenon when J_2 and J_3 are set to one-tenth of their original values while J_1 remains unchanged. As compared to Fig. 1(c), the bottom four bands are compressed towards $E/J_1 = -1$, and the top two bands are compressed towards $E/J_1 = 2$. In particular, the bottom four bands become almost dispersionless like flat bands. This indicates an interesting and feasible approach to realizing flat bands.

To test this approach experimentally, we utilize atomic manipulation to construct kagome-honeycomb lattices with Fe adatoms and investigate their dI/dV spectra at 4.7 K. The Fe adatoms are evaporated on Ag(111) at 6 K within the scanning-tunneling microscope (STM) stage using electron beam evaporation with the typical rate of 0.002 monolayer equivalent per minute. The base pressure of the STM chamber is 2×10^{-11} mbar. Prior to the evaporation, the substrate was cleaned by cycles of sputtering with 2.5 kV Ar^+ ions and annealing at 810 K [47]. Tungsten tips are used and the sample is biased by V_s. The spectroscopy is performed with a modulation of 4–6 mV at 6.7 kHz after stabilizing the tip at 50 mV and 1 nA. Previously, we demonstrated a surface state assisted long-range hopping between the Fe adatoms on Ag(111) [39]. The interatomic distance r dependent hopping term (overlap energy) $J(r)$ between Fe adatoms exhibits a $1/r^2$ dependence. This quantitative information allows us to tune the corresponding hopping between adatoms in the lattices by changing a or b in the kagome-honeycomb lattices.

Figure 2(a) presents a topographic image of a kagome-honeycomb lattice with $a = b = 1.5$ nm assembled by 39 Fe adatoms. With the $1/r^2$ dependence of the hopping term, we readily obtain $J_1 = J_2$ and $J_3 = J_1/3$, which corresponds to the case shown in Fig. 1(c). To minimize the influence of the edge effect, we performed dI/dV measurements on top of the three adatoms placed at the center. We also obtained the spectrum on an isolated Fe adatom, which is placed on a wide terrace and more than 10 nm away from the other adatoms or defects. We took the average value of the dI/dV spectra obtained on top of the central three adatoms, which are almost the same as the theoretical calculation, and it reduces the impact of the slight misplacement of the adatoms (Supplemental Material Note 6 [46]). We further normalized this dI/dV spectrum to that obtained on the isolated Fe adatom to reduce the slight variations of the experimental conditions induced by different tips. The result is plotted in Fig. 2(b). It shows three

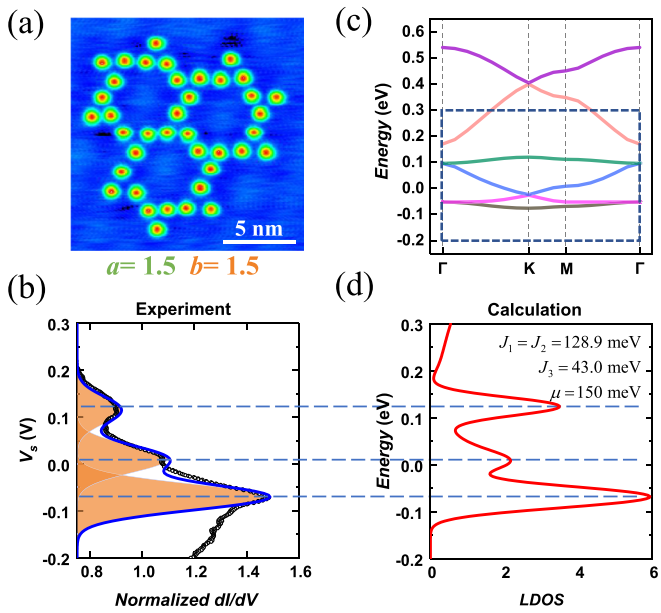

FIG. 2. (a) Topographic image of a kagome-honeycomb lattice with $a = b = 1.5$ nm constructed with 39 Fe adatoms on Ag(111). Imaging parameters: $V_s = -500$ mV, $I = 1$nA. (b) Normalized dI/dV spectrum (black symbols) acquired on top of the central three adatoms. Fitting peaks are marked in orange and their sum is indicated by the blue line. (c) Calculated band structure of the kagome-honeycomb lattice with the parameters shown in the inset of (d). The dashed blue rectangle denotes the energy range used in the experiments. (d) Calculated local density of states (LDOS) with a Gaussian broadening width of 18 meV based on the band structure shown in (c). To better compare the experiments with the theory, three dashed lines are used to connect (b) and (d).

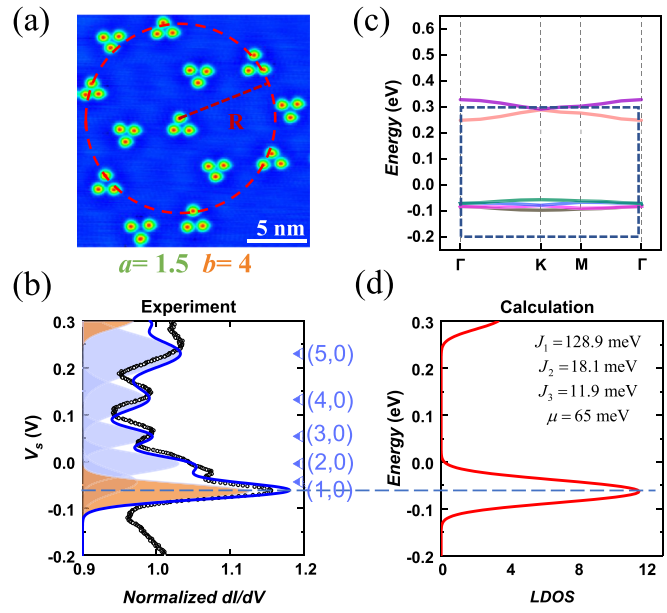

FIG. 3. (a) Topographic image of a kagome-honeycomb lattice with $a = 1.5$ nm and b=4 nm. Imaging parameters: V_s=−500 mV, $I = 1$nA. (b) The black symbols represent the averaged and normalized dI/dV spectrum obtained on top of the central three adatoms. The blue triangles on the right denote the positions of the corresponding interference states (see Supplemental Material Note 3 [46]) with the corresponding quantum numbers. The lattice's characteristic fitting peaks are shaded in orange while additional peaks induced by the interference states are shaded in light blue. The blue line indicates the sum of the peaks. (c), (d) Tight-binding calculated band structure and LDOS of the lattice with the corresponding hopping terms and on-site energy marked in the inset of (d).

pronounced peaks, located at $V_s = -70.8$, 10.4, and 115.0 mV, respectively. To understand the underlying physics, we performed tight-binding calculations with more realistic values. Previously, we found that the effective overlap energy can be quantitatively described by $J(r) = C_\Delta/r^2$ with $C_\Delta = 274 \pm 15\,\text{meV nm}^2$ for Fe adatoms placed with r in between 1.5 and 4.8 nm [39]. With this dependence, we derived J_1, J_2, and J_3, and used them to calculate the corresponding band structure as well as the LDOS, where 18 meV Gaussian broadening was used. The obtained LDOS shows a close similarity to the experimentally obtained spectroscopy. With the fine-tuning values of $C_\Delta = 290\,\text{meV nm}^2$ and $\mu_i = 150$ meV, the calculated LDOS reproduces all the experimental peak positions, including the three featured peaks, which are highlighted by the blue dashed lines connecting Figs. 2(b) and 2(d). In addition, the sum of the three Gaussian peaks, the solid blue line in Fig. 2(b), essentially reproduces the measured dI/dV spectrum very well except in the energy range below −0.1 V. The obtained value of $C_\Delta = 290\,\text{meV nm}^2$ is also in good agreement with the previously obtained one, $274 \pm 15\,\text{meV nm}^2$. Thus, the obtained dI/dV spectrum essentially captures the LDOS features of the kagome-honeycomb lattice. Note that the spectrum cannot be fitted without J_3, where an almost equal separation of these three peaks is expected. This also indicates the strong influence of high-order NN hopping on the band structure and LDOS.

To realize the aforementioned prediction of the band compression phenomenon, we experimentally tune the hopping ratio by tailoring the kagome-honeycomb lattice shape, where we increase b to 4 nm and keep $a = 1.5$ nm unchanged. Figure 3(a) shows the topographic image of the assembled agome-honeycomb lattice. Applying the same value of $C_\Delta = 290\,\text{meV nm}^2$, we obtain $J_1 = 128.9$ meV, $J_2 \approx 0.14J_1$, and $J_3 \approx 0.09J_1$ for this particular geometry. These hopping terms are used to calculate the corresponding band structure as well as the LDOS with the results shown in Figs. 3(c) and 3(d), respectively. In comparison with Fig. 2, the band compression effect is evident in the calculation as only two characteristic peaks are present. The experimentally obtained dI/dV spectrum [Fig. 3(b)], however, shows more than two peaks in contrast to the calculation. A comparison reveals that the experimental spectrum contains the lattice's characteristic peaks (orange) as well as a series of additional peaks (light blue). The two peaks in the orange match well with the calculated ones when we set $\mu = 65$ meV, indicating the band compression effect. These extra peaks may originate from the interference effect caused by the surrounding adatoms. When some adatoms are distributed at an equal distance from the probed adatom, the scattered electron waves by these adatoms may form a constructive phase that contributes peaks similar to the quantum well states due to the interference [48–50]. Taking a close look at the lattice structure, we indeed find

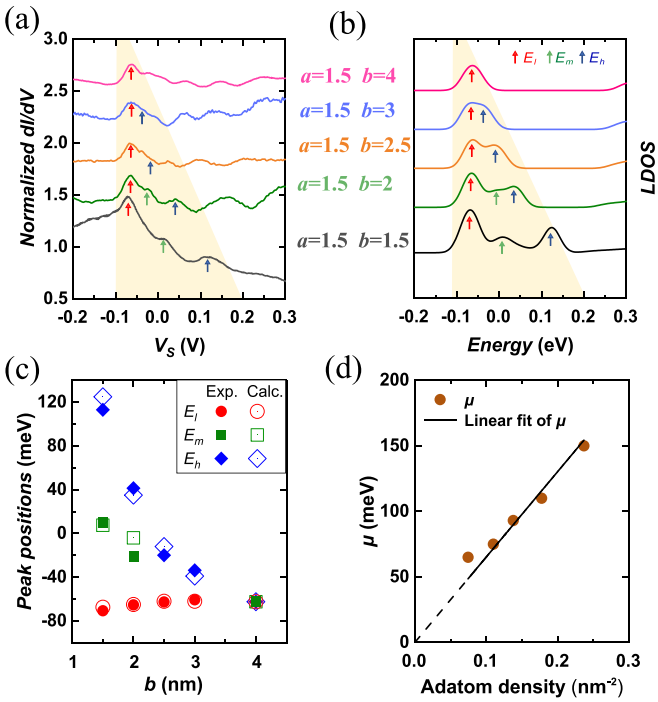

FIG. 4. (a), (b) Normalized differential conductance spectra (left) and the calculated LDOS (right) of a series of kagome-honeycomb lattices with different b. Red, green, and blue arrows mark the low-, middle-, and high-energy peaks, respectively. The spectra are shifted vertically for clarity. (c) The comparison between the experimentally obtained and the theoretically calculated peak positions. (d) The fitted on-site energy as a function of the Fe adatom density.

that several outer adatoms of the structure are located with almost an equal separation of ∼9.6 nm, highlighted by the dashed red circle shown in Fig. 3(a). We calculated the energy levels of the corresponding interference states and marked them with the corresponding quantum numbers in Fig. 3(b). Remarkably, we found that the calculated positions of the interference states are close to the additional peaks in the experimentally obtained dI/dV spectrum (see Supplemental Material Note 3 [46]). In order to further confirm this, we also experimentally built the structures with the adatoms at the marked circle and one at the center. The obtained dI/dV spectrum on top of the center adatom essentially reproduced these peaks (Supplemental Material Note 4 [46]), confirming their quantum interference origin. The sum of the lattice-induced LDOS peaks (orange) and the effective quantum-interference-induced peaks (light blue) matches well with the experimental spectrum. Such excellent one-to-one correspondence strongly implies the novel band compression effect. In Supplemental Material Note 3 [46], we also provided a possible explanation why the interference states were not observed in Fig. 2(b).

To further visualize the band structure evolution with the high-order hopping term and to demonstrate the band compression effect, we assembled a series of kagome-honeycomb lattices with various b but the same a. Their measured dI/dV spectra are listed in Fig. 4(a) for five different b/a, where we focus on the first three characteristic peaks of the lattices, namely, the area marked by orange. The presence of other peaks could be relevant to the interference effect of their surrounding adatoms, similar to that discussed in Fig. 3. When $b/a = 1$, the spectrum shows three well-separated peaks denoted by the low-energy peak E_l (red arrow), middle-energy peak E_m (green arrow), and high-energy peak E_h (blue arrow), respectively. With increasing b/a, the low-energy peak exhibits a blueshift towards higher energy while the middle- and high-energy peaks show redshifts towards lower energy. When $b/a \approx 1.67$, the middle-energy peak is hardly visible. And the three peaks merge into a broad feature when $b = 2$. Importantly, the three peaks merge into one with a relatively narrow width when $b/a = 2.67$, suggesting the band compression effect. For comparison, we calculate the LDOS using the tight-binding method with the corresponding hopping terms, where we take the same value of $C_\Delta = 290\,\text{meV nm}^2$ and utilize $J_1 = C_\Delta/a^2$, $J_2 = C_\Delta/b^2$, and $J_3 = C_\Delta/[(b + a/2)^2 + a^2/4]$ to derive the corresponding hopping terms. To match the positions of the calculated peaks with the experimental ones, we also use one single fitting parameter, the on-site energy, μ, which only shifts the entire calculated LDOS upwards or downwards. The variation of μ with the different lattices will be discussed in the next paragraph. The calculated LDOS of the lattices corresponding to the experimental ones are plotted in Fig. 4(b). Remarkably, we find that the calculated LDOS have similar shapes with the experimentally obtained normalized dI/dV spectra, especially on the peak positions. Note the peak intensity of the normalized dI/dV not only reflects the information of the LDOS on the sample but also contains the information on the tip and the tunneling gap [51–53], which may affect the agreement of the peak intensities. To obtain the quantitative information, we plotted both the experimentally obtained peak positions and the theoretically calculated ones of all three peaks in one figure. As shown in Fig. 4(c), they are almost identical within the error margins. The excellent one-to-one correspondence between the experiments and the tight-binding calculations unambiguously demonstrates the merging of these peaks with the decreasing of the ratio of high-order NN hopping with respect to the first NN hopping, namely, the band compression effect.

Last, we discuss the evolution of μ with the lattice parameters. In the above discussions, we need to implant a different μ to align the calculated LDOS with the experimentally obtained spectrum for each lattice with different b. We find that μ exhibits a nonlinear dependence with b. Noticing that the density of the Fe adatom lattice changes when b is varied, we also plotted μ as the function of the Fe adatom density in Fig. 4(d). Interestingly, we find an almost linear dependence. One would expect the surface to become Ag(111) or Fe(111) when the Fe adatom density reaches zero or the surface atom density of Fe(111), respectively. We extrapolated the slope, which is $0.633\,\text{eV nm}^2$, and multiplied it by the surface atom density of Fe(111). The obtained value is ∼50 times larger than the difference between the reported values of Fe(111) and Ag(111) surfaces [54], which might be related to the structural and elastic difference between a monolayer Fe(111) on Ag(111) crystal and a (111) surface of bulk Fe crystal. Nevertheless, the comparison between the experimental and theoretical peak positions can serve as a good estimation of the on-site energy.

III. SUMMARY

In summary, we have constructed a series of kagome-honeycomb lattices with Fe adatoms on the Ag(111) surface and investigated their lattice parameter dependent dI/dV spectra. Using lattice engineering, we find that the probed spectra exhibit the characteristic peaks of the lattices and they merge into one peak with increasing the ratio of the high-order NN and first NN distances. With previously obtained interatomic distance-dependent hopping terms, the tight-binding method based LDOS calculation shows one-to-one correspondence with the experimental dI/dV spectra on the peak positions. Our findings reveal the important role of the high-order NN hopping terms on the electronic band structure. Importantly, both the experiments and theoretical calculations unambiguously demonstrate the band compression effect. We note that the band compression effect is not the simple band width shrinking with decreasing the interatomic hopping as pointed out in Supplemental Material Note 7 [46]. The band compression effect also provides an alternative approach to pursuing the flat band. The ability to generate dispersionless flat bands utilizing band compression makes artificial structures a fertile platform to realize the exotic many-body phenomena, such as the Hofstadter butterfly [55–57] or Wigner crystallization [58–60].

ACKNOWLEDGMENTS

This work was supported by the National Key R&D Program of China (Grants No. 2022YFA1403601 and No. 2018YFA0306004) and the National Natural Science Foundation of China (Grants No. 11974165, No. 92165103, No. 51971110, No. 12274203, No. 12274204, and No. 12241402). We sincerely appreciate the valuable discussions with Y. M. Dai.

[1] D. Leykam, A. Andreanov, and S. Flach, Artificial flat band systems: From lattice models to experiments, Adv. Phys.-X **3**, 1473052 (2018).

[2] E. J. Bergholtz and Z. Liu, Topological flat band models and fractional Chern insulators, Int. J. Mod. Phys. B **27**, 1330017 (2013).

[3] S. Q. Deng, A. Simon, and J. Kohler, The origin of a flat band, J. Solid State Chem. **176**, 412 (2003).

[4] H. S. Nguyen, F. Dubois, T. Deschamps, S. Cueff, A. Pardon, J. L. Leclercq, C. Seassal, X. Letartre, and P. Viktorovitch, Symmetry Breaking in Photonic Crystals: On-Demand Dispersion from Flatband to Dirac Cones, Phys. Rev. Lett. **120**, 066102 (2018).

[5] E. H. Lieb, Two Theorems on the Hubbard Model, Phys. Rev. Lett. **62**, 1201 (1989).

[6] H. Tasaki, Ferromagnetism in the Hubbard Models with Degenerate Single-Electron Ground States, Phys. Rev. Lett. **69**, 1608 (1992).

[7] H. Tasaki, Stability of Ferromagnetism in the Hubbard Model, Phys. Rev. Lett. **73**, 1158 (1994).

[8] H. Liu, G. Sethi, D. N. Sheng, Y. N. Zhou, J. T. Sun, S. Meng, and F. Liu, High-temperature fractional quantum Hall state in the Floquet kagome flat band, Phys. Rev. B **105**, L161108 (2022).

[9] E. Tang, J. W. Mei, and X. G. Wen, High-Temperature Fractional Quantum Hall States, Phys. Rev. Lett. **106**, 236802 (2011).

[10] G. Chen, A. L. Sharpe, P. Gallagher, I. T. Rosen, E. J. Fox, L. Jiang, B. Lyu, H. Li, K. Watanabe, T. Taniguchi, J. Jung, Z. Shi, D. Goldhaber-Gordon, Y. Zhang, and F. Wang, Signatures of tunable superconductivity in a trilayer graphene moire superlattice, Nature (London) **572**, 215 (2019).

[11] Z. Hao, A. M. Zimmerman, P. Ledwith, E. Khalaf, D. H. Najafabadi, K. Watanabe, T. Taniguchi, A. Vishwanath, and P. Kim, Electric field–tunable superconductivity in alternating-twist magic-angle trilayer graphene, Science **371**, 1133 (2021).

[12] Y. Cao, V. Fatemi, A. Demir, S. Fang, S. L. Tomarken, J. Y. Luo, J. D. Sanchez-Yamagishi, K. Watanabe, T. Taniguchi, E. Kaxiras, R. C. Ashoori, and P. Jarillo-Herrero, Correlated insulator behaviour at half-filling in magic-angle graphene superlattices, Nature (London) **556**, 80 (2018).

[13] Y. Cao, V. Fatemi, S. Fang, K. Watanabe, T. Taniguchi, E. Kaxiras, and P. Jarillo-Herrero, Unconventional superconductivity in magic-angle graphene superlattices, Nature (London) **556**, 43 (2018).

[14] L. Wang, E. M. Shih, A. Ghiotto, L. Xian, D. A. Rhodes, C. Tan, M. Claassen, D. M. Kennes, Y. Bai, B. Kim, K. Watanabe, T. Taniguchi, X. Zhu, J. Hone, A. Rubio, A. N. Pasupathy, and C. R. Dean, Correlated electronic phases in twisted bilayer transition metal dichalcogenides, Nat. Mater. **19**, 861 (2020).

[15] F. Steglich and S. Wirth, Foundations of heavy-fermion superconductivity: Lattice Kondo effect and Mott physics, Rep. Prog. Phys. **79**, 084502 (2016).

[16] R. H. Zhang, H. Y. Ren, and L. He, Flat bands and related novel quantum states in two-dimensional systems, Acta Phys. Sin. **71**, 127302 (2022).

[17] Y. Zhang, Z. Jiang, J. P. Small, M. S. Purewal, Y. W. Tan, M. Fazlollahi, J. D. Chudow, J. A. Jaszczak, H. L. Stormer, and P. Kim, Landau-Level Splitting in Graphene in High Magnetic Fields, Phys. Rev. Lett. **96**, 136806 (2006).

[18] J. Mao, S. P. Milovanovic, M. Andelkovic, X. Lai, Y. Cao, K. Watanabe, T. Taniguchi, L. Covaci, F. M. Peeters, A. K. Geim, Y. Jiang, and E. Y. Andrei, Evidence of flat bands and correlated states in buckled graphene superlattices, Nature (London) **584**, 215 (2020).

[19] R. Xu, L. J. Yin, J. B. Qiao, K. K. Bai, J. C. Nie, and L. He, Direct probing of the stacking order and electronic spectrum of rhombohedral trilayer graphene with scanning tunneling microscopy, Phys. Rev. B **91**, 035410 (2015).

[20] Z. Li, J. Zhuang, L. Wang, H. Feng, Q. Gao, X. Xu, W. Hao, X. Wang, C. Zhang, K. Wu, S. X. Dou, L. Chen, Z. Hu, and Y. Du, Realization of flat band with possible nontrivial topology in electronic Kagome lattice, Sci. Adv. **4**, aau4511 (2018).

[21] H. M. Yu, S. Sharma, S. Agarwal, O. Liebman, and A. S. Banerjee, Carbon kagome nanotubes—quasi-one-dimensional nanostructures with flat bands, arXiv:2301.10200.

[22] T. Neupert, L. Santos, C. Chamon, and C. Mudry, Fractional Quantum Hall States at Zero Magnetic Field, Phys. Rev. Lett. **106**, 236804 (2011).
[23] B. Sutherland, Localization of electronic wave functions due to local topology, Phys. Rev. B **34**, 5208 (1986).
[24] D. N. Sheng, Z. C. Gu, K. Sun, and L. Sheng, Fractional quantum Hall effect in the absence of Landau levels, Nat. Commun. **2**, 389 (2011).
[25] K. Sun, Z. Gu, H. Katsura, and S. Das Sarma, Nearly Flatbands with Nontrivial Topology, Phys. Rev. Lett. **106**, 236803 (2011).
[26] S. Okamoto, N. Mohanta, E. Dagotto, and D. N. Sheng, Topological flat bands in a kagome lattice multiorbital system, Commun. Phys. **5**, 198 (2022).
[27] K. Ohgushi, S. Murakami, and N. Nagaosa, Spin anisotropy and quantum Hall effect in the *kagomé* lattice: Chiral spin state based on a ferromagnet, Phys. Rev. B **62**, R6065 (2000).
[28] T. Bilitewski and R. Moessner, Disordered flat bands on the kagome lattice, Phys. Rev. B **98**, 235109 (2018).
[29] M. G. Kang, S. A. Fang, J. K. Kim, B. R. Ortiz, S. H. Ryu, J. M. Kim, J. Yoo, G. Sangiovanni, D. Di Sante, B. G. Park, C. Jozwiak, A. Bostwick, E. Rotenberg, E. Kaxiras, S. D. Wilson, J. H. Park, and R. Comin, Twofold van Hove singularity and origin of charge order in topological kagome superconductor CsV_3Sb_5, Nat. Phys. **18**, 301 (2022).
[30] M. Kang, L. Ye, S. Fang, J. S. You, A. Levitan, M. Han, J. I. Facio, C. Jozwiak, A. Bostwick, E. Rotenberg, M. K. Chan, R. D. McDonald, D. Graf, K. Kaznatcheev, E. Vescovo, D. C. Bell, E. Kaxiras, J. van den Brink, M. Richter, M. Prasad Ghimire *et al.*, Dirac fermions and flat bands in the ideal kagome metal FeSn, Nat. Mater. **19**, 163 (2020).
[31] H. Huang, L. Zheng, Z. Lin, X. Guo, S. Wang, S. Zhang, C. Zhang, Z. Sun, Z. Wang, H. Weng, L. Li, T. Wu, X. Chen, and C. Zeng, Flat-Band-Induced Anomalous Anisotropic Charge Transport and Orbital Magnetism in Kagome Metal CoSn, Phys. Rev. Lett. **128**, 096601 (2022).
[32] Z. Lin, J. H. Choi, Q. Zhang, W. Qin, S. Yi, P. Wang, L. Li, Y. Wang, H. Zhang, Z. Sun, L. Wei, S. Zhang, T. Guo, Q. Lu, J. H. Cho, C. Zeng, and Z. Zhang, Flatbands and Emergent Ferromagnetic Ordering in Fe_3Sn_2 Kagome Lattices, Phys. Rev. Lett. **121**, 096401 (2018).
[33] M. Fu, T. Imai, T. H. Han, and Y. S. Lee, Evidence for a gapped spin-liquid ground state in a kagome Heisenberg antiferromagnet, Science **350**, 655 (2015).
[34] L. Ye, M. Kang, J. Liu, F. von Cube, C. R. Wicker, T. Suzuki, C. Jozwiak, A. Bostwick, E. Rotenberg, D. C. Bell, L. Fu, R. Comin, and J. G. Checkelsky, Massive Dirac fermions in a ferromagnetic kagome metal, Nature (London) **555**, 638 (2018).
[35] M. Li, Q. Wang, G. Wang, Z. Yuan, W. Song, R. Lou, Z. Liu, Y. Huang, Z. Liu, H. Lei, Z. Yin, and S. Wang, Dirac cone, flat band and saddle point in kagome magnet YMn_6Sn_6, Nat. Commun. **12**, 3129 (2021).
[36] R. Drost, T. Ojanen, A. Harju, and P. Liljeroth, Topological states in engineered atomic lattices, Nat. Phys. **13**, 668 (2017).
[37] K. K. Gomes, W. Mar, W. Ko, F. Guinea, and H. C. Manoharan, Designer Dirac fermions and topological phases in molecular graphene, Nature (London) **483**, 306 (2012).
[38] M. R. Slot, T. S. Gardenier, P. H. Jacobse, G. C. P. van Miert, S. N. Kempkes, S. J. M. Zevenhuizen, C. M. Smith, D. Vanmaekelbergh, and I. Swart, Experimental realization and characterization of an electronic Lieb lattice, Nat. Phys. **13**, 672 (2017).
[39] X. X. Li, Q. L. Li, T. Z. Ji, R. G. Yan, W. L. Fan, B. F. Miao, L. Sun, G. Chen, W. Y. Zhang, and H. F. Ding, Lieb lattices formed by real atoms on Ag(111) and their lattice constant-dependent electronic properties, Chin. Phys. Lett. **39**, 057301 (2022).
[40] S. Sun, S. Zhao, Y. Z. Luo, X. Gu, X. Lian, A. Tadich, D. C. Qi, Z. Ma, Y. Zheng, C. Gu, J. L. Zhang, Z. Li, and W. Chen, Designing Kagome lattice from potassium atoms on phosphorus–gold surface alloy, Nano Lett. **20**, 5583 (2020).
[41] M. Telychko, G. Li, P. Mutombo, D. Soler-Polo, X. Peng, J. Su, S. Song, M. J. Koh, M. Edmonds, P. Jelinek, J. Wu, and J. Lu, Ultrahigh-yield on-surface synthesis and assembly of circumcoronene into a chiral electronic Kagome-honeycomb lattice, Sci. Adv. **7**, abf0269 (2021).
[42] W. X. Qiu, S. Li, J. H. Gao, Y. Zhou, and F. C. Zhang, Designing an artificial Lieb lattice on a metal surface, Phys. Rev. B **94**, 241409(R) (2016).
[43] H. Takeda, T. Takashima, and K. Yoshino, Flat photonic bands in two-dimensional photonic crystals with kagome lattices, J. Phys.: Condens. Matter **16**, 6317 (2004).
[44] J. Ibanez-Azpiroz, A. Eiguren, A. Bergara, G. Pettini, and M. Modugno, Tight-binding models for ultracold atoms in honeycomb optical lattices, Phys. Rev. A **87**, 011602(R) (2013).
[45] C. Barreteau, F. Ducastelle, and T. Mallah, A bird's eye view on the flat and conic band world of the honeycomb and Kagome lattices: Towards an understanding of 2D metal-organic frameworks electronic structure, J. Phys.: Condens. Matter **29**, 465302 (2017).
[46] See Supplemental Material at http://link.aps.org/supplemental/10.1103/PhysRevB.108.075153 for tight-binding calculations of the influence of Fe adatom misplacements on LDOS.
[47] Q. Li, X. Li, B. Miao, L. Sun, G. Chen, P. Han, and H. Ding, Kondo-free mirages in elliptical quantum corrals, Nat. Commun. **11**, 1400 (2020).
[48] Q. L. Li, R. X. Cao, and H. F. Ding, Quantum size effect in nanocorrals: From fundamental to potential applications, Appl. Phys. Lett **117**, 060501 (2020).
[49] R. X. Cao, Z. Liu, B. F. Miao, L. Sun, D. Wu, B. You, S. C. Li, W. Zhang, A. Hu, S. D. Bader, and H. F. Ding, Self-regulated Gd atom trapping in open Fe nanocorrals, Phys. Rev. B **90**, 045433 (2014).
[50] Q. L. Li, C. Zheng, R. Wang, B. F. Miao, R. X. Cao, L. Sun, D. Wu, Y. Z. Wu, S. C. Li, B. G. Wang, and H. F. Ding, Role of the surface state in the Kondo resonance width of a Co single adatom on Ag(111), Phys. Rev. B **97**, 035417 (2018).
[51] C. J. Chen, *Introduction to Scanning Tunneling Microscopy* (Oxford University Press, New York, 2007).
[52] H. J. Zandvliet and A. van Houselt, Scanning tunneling spectroscopy, Annu. Rev. Anal. Chem. **2**, 37 (2009).
[53] D. Bonnell, *Scanning Tunneling Microscopy and Spectroscopy: Theory, Techniques, and Applications* (Wiley-VCH, New York, 2001).
[54] L. Vitos, A. V. Ruban, H. L. Skriver, and J. Kollar, The surface energy of metals, Surf. Sci. **411**, 186 (1998).
[55] B. Hunt, J. D. Sanchez-Yamagishi, A. F. Young, M. Yankowitz, B. J. LeRoy, K. Watanabe, T. Taniguchi, P. Moon, M. Koshino,

P. Jarillo-Herrero, and R. C. Ashoori, Massive Dirac fermions and Hofstadter butterfly in a van der Waals heterostructure, Science **340**, 1427 (2013).

[56] P. Roushan, C. Neill, J. Tangpanitanon, V. M. Bastidas, A. Megrant, R. Barends, Y. Chen, Z. Chen, B. Chiaro, A. Dunsworth, A. Fowler, B. Foxen, M. Giustina, E. Jeffrey, J. Kelly, E. Lucero, J. Mutus, M. Neeley, C. Quintana, D. Sank *et al.*, Spectroscopic signatures of localization with interacting photons in superconducting qubits, Science **358**, 1175 (2017).

[57] T. Fabian, M. Kausel, L. Linhart, J. Burgdorfer, and F. Libisch, Half-integer Wannier diagram and Brown-Zak fermions of graphene on hexagonal boron nitride, Phys. Rev. B **106**, 165412 (2022).

[58] H. Li, S. Li, E. C. Regan, D. Wang, W. Zhao, S. Kahn, K. Yumigeta, M. Blei, T. Taniguchi, K. Watanabe, S. Tongay, A. Zettl, M. F. Crommie, and F. Wang, Imaging two-dimensional generalized Wigner crystals, Nature (London) **597**, 650 (2021).

[59] Y. Zhou, J. Sung, E. Brutschea, I. Esterlis, Y. Wang, G. Scuri, R. J. Gelly, H. Heo, T. Taniguchi, K. Watanabe, G. Zarand, M. D. Lukin, P. Kim, E. Demler, and H. Park, Bilayer Wigner crystals in a transition metal dichalcogenide heterostructure, Nature (London) **595**, 48 (2021).

[60] T. Smolenski, P. E. Dolgirev, C. Kuhlenkamp, A. Popert, Y. Shimazaki, P. Back, X. Lu, M. Kroner, K. Watanabe, T. Taniguchi, I. Esterlis, E. Demler, and A. Imamoglu, Signatures of Wigner crystal of electrons in a monolayer semiconductor, Nature (London) **595**, 53 (2021).